Politecnico di Torino

Politecnico di Torino

MSc in Communication and Computer Networks Engineering

Numerical investigations on the connection between surface waves and trasmitting properties of tunable periodic structures

Supervisors: Prof. Ladislau Matekovits

Candidate: Christian Palma

Academic Year 2023/24

Contents

Chapter 1

Introduction

1.1 Topic Overview

In the landscape of modern telecommunications, advanced technologies based on Periodic structures such as Metamaterials and Tunable Frequency Selective Surfaces (TFSS) are playing an increasingly crucial role. These technologies offer new possibilities for controlling and manipulating electromagnetic (EM) waves, significantly enhancing the performance of communication systems [1, 2].
Periodic structures are formed by elements that repeat regularly in space, called unit cells, and can be designed in one-dimensional (1D), two-dimensional (2D), or three-dimensional (3D) configurations. This periodicity gives these structures unique properties, such as band gaps, which prevent the propagation of EM waves at certain frequencies. In telecommunications, these properties can be exploited to create advanced filters and waveguides [3].
The main difference when it comes to metamaterials and FSS concerns the angle of incidence at which the periodic structure is excited. FSS is considered as when a periodic structure is excited by an impacting wave arriving from a non-grazing angle, i.e., from an angle of incidence other than 90° to the normal to the surface. Viceversa, a metamaterial is considered as when a periodic structure is excited by an impacting wave from a grazing angle, i.e., 90° to the surface normal [4].
Metamaterials are artificial materials designed to achieve EM properties not found in nature. These materials rely on sub-wavelength resonant structures, allowing for advanced control of EM waves. One of the most revolutionary features is the negative refractive index, which enables the creation of super-resolution lenses and devices for manipulating waves in innovative ways. In telecommunications, metamaterials can be employed to develop more efficient and compact antennas capable of operating over broader frequency bands with lower signal loss. Additionally, they can be used to create cloaking devices that can hide antennas and other devices from radar, enhancing the security and discretion of installations [5].
TFSS are surfaces capable of selectively transmitting or reflecting EM waves based on frequency. Their tunability, or the ability to dynamically modify their frequency selective properties, makes them particularly suitable for advanced applications in telecommunications. They can be designed using resonant elements such as rings or patches, of which resonant frequency can be adjusted through external stimuli like electric fields, magnetic fields, or temperature changes. For example, using varactors or PIN diodes allows for the variation of the resonators' capacitances, thus altering the surface's frequency response. This tunability enables to be used as adjustable filters for antennas, improving signal selectivity and reducing interference [2]. Ad-

ditionally, in defense applications, they can be used to create adaptive absorbing surfaces that reduce the radar signature of vehicles or installations, increasing their invisibility to detection systems [6].

1.2 Target

The objective of this thesis was to do a numerical investigation and analysis of surface waves in relation to the transmission properties of tunable periodic structures, so that they can be used in the future advancement of wireless technology. For this purpose, a unit cell was designed on which numerical simulations were carried out using CST Studio Suite Academic [20], a tool well suited for the study of periodic structures. In particular, the aim of this thesis work focused on the correlation between the propagation of surface waves modes to periodic structures and the angle of incidence that excites it. Therefore, an in-depth analysis was conducted on the modes propagating on the surface, both in terms of Dispersion Diagram (DD) and Scattering parameters.

1.3 Structure of the thesis

The thesis was organized into five chapters.
The first chapter was aimed at offering a brief and concise introduction of the subject matter. The second chapter was intended to provide the reader with an overview of the basic literature needed to study the phenomenon addressed in this thesis. The main topics that were covered were mainly Periodic Structures and their characteristics, Metamaterials, Frequency Selective Surface (FSS), and a brief introduction related to DD. The third chapter was aimed at detailing all the steps necessary to design the unit cell and its different configurations analyzed. In addition, a section was devoted to describe the configurations set to start the simulations. In the fourth chapter, the results obtained were exposed and extensively described. Finally, possible future work and applicable improvements were proposed in the fifth chapter.

Chapter 2

Review of Literature

2.1 Periodic structures

Humans have always been fascinated by symmetry and periodicity, and there were many examples of these kinds of structures in nature, including crystals and buildings. In terms of physics, periodicity denotes simplicity and ease of expression and description through mathematical formulas, while symmetry denotes stability and minimal energy. The best known example is the mathematical description of periodic waves provided by Floquet or Bloch functions, which are in fact the same functions applied in different domains. In fact, we understood that all functions, even those characterizing material properties, could be written as a set of periodic functions such as sine or cosine functions in the Cartesian system. The periodic arrangement of atoms or structures was the source of many physical properties and features, including (electronic) bandgap, EM bandgap (EBG), photonic bandgap, passband/stopband of frequency selective surfaces (FSS), and optical properties of crystals. Therefore, the qualities of both natural materials and manufactured constructions greatly depended on the periodic structure.
The literature has consistently shown interest in the class of periodic structures. In the past, the primary focus was on using 1D periodic structures to guide and scatter waves. Specifically, periodic structures have been used in the microwave field for a wide range of applications. A few examples include phase-array antennas, linear accelerators, filters, artificial dielectrics, phase-wave structures in microwave tubes, linear accelerators, frequency-selective structures, leakywave antennas, and so forth. The computational and experimental investigations of wave phenomena related to 2D and 3D structures have received a lot of interest in the past few years, and numerous applications have been shown [7]. In Figure 2.1 an example of 1D, 2D, and 3D periodic structure was proposed.

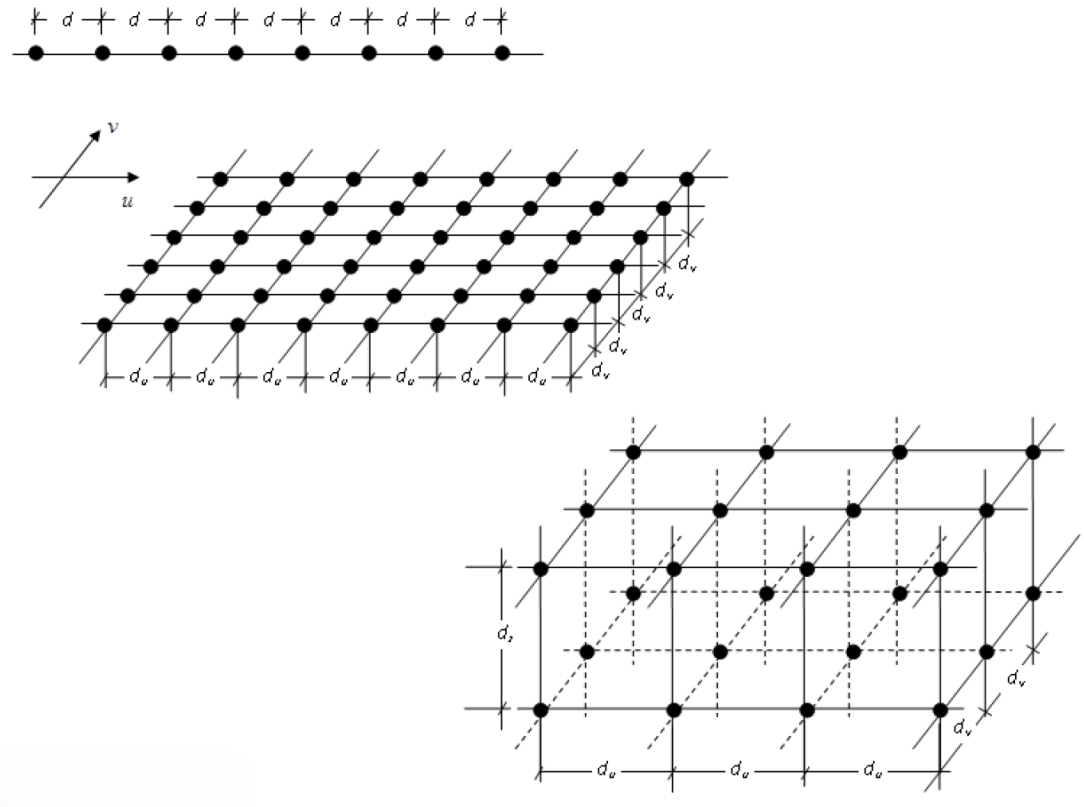

Figure 2.1: Example of 1D, 2D, and 3D periodic structure

Geometric arrangements referred to as periodic structures repeat a fundamental unit, also called a "elementary cell" or "unit cell," in one or more spatial directions (in Fig. 2.1, the unit cell is represented by a single point). The structures' distinctive qualities are a result of their periodicity, which also allows them to control the way EM waves propagate, which are subject to diffraction, transmission, and reflection. Periodic structures have unique EM properties due to their repetitive geometry. This behavior can be understood by analyzing Maxwell's equations in periodic contexts, which govern the behavior of electric and magnetic fields. In presence of a periodic structure, these equations must be solved considering the boundary conditions imposed by the periodicity [8].

2.1.1 Maxwell's Equations and Boundary Condition

The Maxwell's equations (phasorial form) for an EM field in the general case are:

$$\nabla \times \mathbf{E} = -\frac{\partial \mathbf{B}}{\partial t} \tag{2.1}$$

$$\nabla \times \mathbf{H} = \mathbf{J} + \frac{\partial \mathbf{D}}{\partial t} \tag{2.2}$$

$$\nabla \cdot \mathbf{D} = \rho \tag{2.3}$$

$$\nabla \cdot \mathbf{B} = 0 \tag{2.4}$$

where $\mathbf{E}$ is the electric field, $\mathbf{H}$ is the magnetic field, $\mathbf{D}$ is the electric displacement vector, and $\mathbf{B}$ is the magnetic induction vector. The quantities ρ and $\mathbf{J}$ are the volume charge density and electric current density of any external charges [9], respectively.

Boundary conditions are derived from the fundamental laws of electromagnetism and ensure the continuity, are essential for solving Maxwell's equations and proper interaction of EM fields at the boundaries of different media. They are fundamental for three main reasons:
-Solving Maxwell's Equations: proper boundary conditions are necessary to uniquely solve Maxwell's equations for a given physical scenario.
-Determining Field Behavior: they dictate how EM fields behave at interfaces between different materials, which is crucial for understanding phenomena such as reflection, refraction, and transmission of waves.
-Designing EM Devices: they are essential in the design and analysis of a wide range of devices, including antennas, waveguides, and optical fibers [10].

1. Continuity of the tangential component of the electric field:

$$\mathbf{E}_{1t} = \mathbf{E}_{2t} \tag{2.5}$$

   This boundary condition is derived from Faraday's Law by integrating over an infinitesimal loop straddling the boundary, we find that the tangential component of the electric field must be continuous across the boundary.

2. Continuity of the tangential component of the magnetic field:

$$\mathbf{H}_{1t} = \mathbf{H}_{2t} \tag{2.6}$$

   This boundary condition is derived from the modified Ampère's Law by integrating over an infinitesimal loop across the boundary, we find that the tangential component of the magnetic field must be continuous across the boundary, assuming no surface current density at the boundary.

3. Continuity of the normal component of the electric displacement field:

$$\mathbf{D}_{1n} = \mathbf{D}_{2n} \tag{2.7}$$

   This condition is derived from Gauss's Law for electricityb by integrating over a pillbox-shaped region straddling the boundary, the flux of the electric displacement field must be continuous across the boundary, assuming no surface charge density.

4. Continuity of the normal component of the magnetic induction field:

$$\mathbf{B}_{1n} = \mathbf{B}_{2n} \tag{2.8}$$

   This condition is derived from Gauss's Law for magnetism by integrating for magnetism over a pillbox-shaped region, the flux of the magnetic induction field must be continuous across the boundary, reflecting the absence of magnetic monopoles.

Periodic structures have unique properties due to their proper arrangement. These structures can manipulate EM waves in ways that are not possible with traditional materials. The Bloch conditions describe the solutions of Maxwell's equations. These conditions state that the EM field in a periodic medium can be written as the product of a plane wave and a periodic function.

$$\mathbf{E}(\mathbf{r} + \mathbf{T}) = \mathbf{E}(\mathbf{r})e^{i\mathbf{K}\cdot\mathbf{T}} \tag{2.9}$$

where $\mathbf{T}$ is the lattice translation vector, and $\mathbf{K}$ is the wave vector. Bloch conditions simplify the problem by allowing the use of a single unit cell rather than the entire infinite structure for its numerical analysis. This significantly reduces the computational complexity and facilitates the analysis of the EM properties [3].

2.2 Introduction on Metamaterials

The use of artificial structures and composite materials that either replicate well-known material responses or qualitatively have novel, physically realizable response functions that are either uncommon or difficult to find in nature has gained popularity in recent years. These metamaterials' non-traditional response functions are frequently produced by man-made inclusions or inhomogeneities that are incorporated into a host medium, attached to, or implanted on a host surface. Such metamaterials have been anticipated to exhibit exotic characteristics, and several experiments have validated our fundamental knowledge of many of them. The capacity to manipulate a material's optical and EM characteristics for a range of applications is the fundamental attraction of metamaterials. If the wave characteristics can be tailored and manipulated, it might lead to considerable reductions in the size and weight of devices, systems, and components, as well as improvements in their performance. This could have a huge impact. The search for synthetic materials for use in EM fields is not new. This activity has a lengthy history that began with experiments conducted by Jadagis Chunder Bose in 1898 on manufactured twisted materials that display what are now known as chiral features. Karl Ferdinand Lindman investigated wave interaction with sets of metallic helices as synthetic chiral media early in the 20th century. In the 1950s and 1960s, for instance, artificial dielectrics were investigated for use in lightweight microwave antenna lenses. In the 1980s and 1990s, a lot of research was done on artificial chiral materials for use as microwave radar absorbers and other uses [11].

2.3 Frequency Selective Surface

FSS are specialized structures that consist of periodic arrays of conductive elements. These elements are designed to either transmit or reflect EM waves at specific frequencies, effectively filtering and blocking undesired ones [12]. They are excited by an impinging wave arriving from a non-grazing angle, i.e., angle of incidence different from 90° with respect to the normal to the surface [4]. Figure 2.2 shows the functionality of the FSS obtained with a complementary self-resonant network.

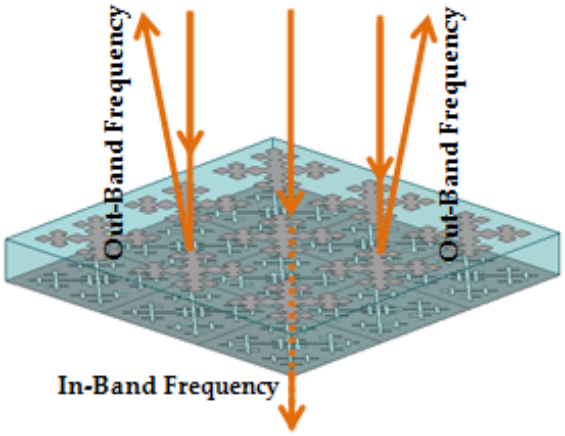

Figure 2.2: FSS functionality [13].

These surfaces leverage resonance to filter EM waves, a principle that enables them to selectively manipulate wave propagation based on the design of their elements [12, 14]. The design of an FSS involves selecting the shape, size, and arrangement of its elements, which can include patches, slots, or dipoles. These elements are typically arranged in a periodic pattern on a dielectric substrate. The geometric parameters and periodicity of these elements determine the resonant frequency and bandwidth of the FSS [2, 15]. FSS are utilized in a variety of applications. In antenna systems, they are used to design radomes that selectively filter frequencies, enhancing signal clarity and reducing interference. In EM shielding, they provide EM compatibility (EMC) by blocking unwanted frequencies while allowing desired signals to pass, protecting electronic devices from interference. In communication systems, they create filters that separate different frequency bands, optimizing bandwidth and minimizing cross-talk. Additionally, in stealth technology, FSS design surfaces that absorb specific frequencies, making objects less detectable by radar systems [16, 17]. TFSS represents an advanced evolution of FSS technology. Unlike static FSS, TFSS can dynamically adjust their resonant frequency in response to external stimuli, such as electrical, mechanical, thermal, or optical changes. This tunability is achieved by integrating active components like varactors, PIN diodes, microelectromechanical systems (MEMS), or materials with variable properties into the FSS structure [2]. An example of a unit cell of an FSS is depicted in Fig. 2.3, while Fig. 2.4 shows the same structure in which PIN diodes are applied, obtaining a TFSS.

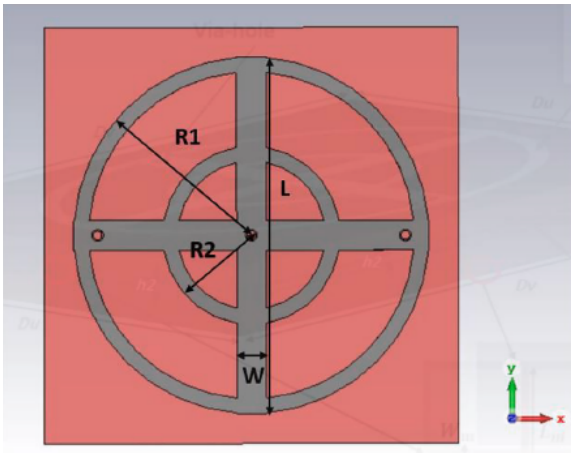

Figure 2.3: Example of unit cell in FSS [4].

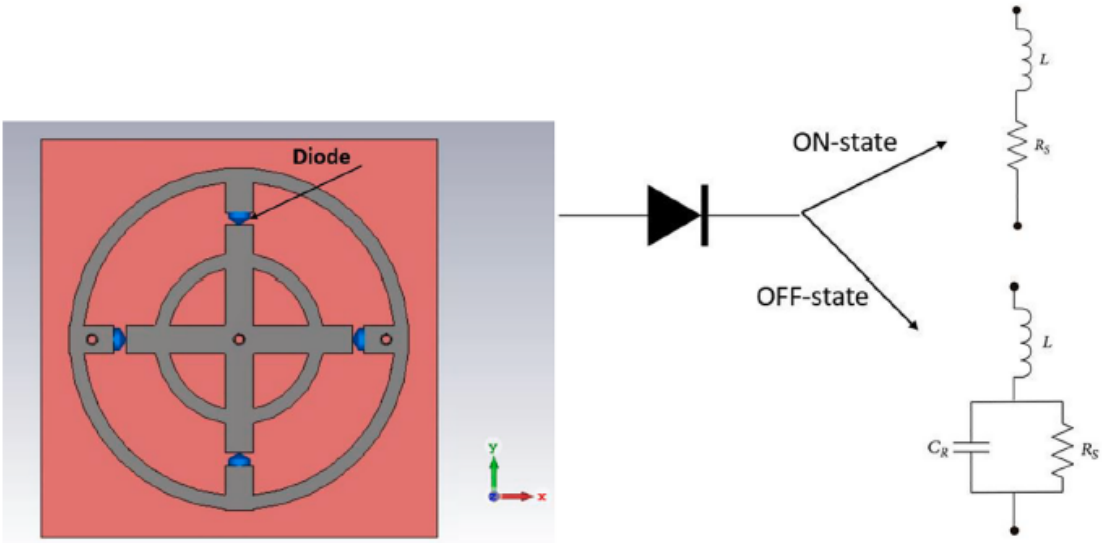

Figure 2.4: TFSS with PIN diode and the equivalent circuit of PIN diode applied in ON and OFF state [4].

2.4 Dispersion Diagram

The DD is a powerful tool for analyzing periodic structures and can be used to verify the left-handed properties of materials. This diagram characterizes the behavior of EM waves in periodic structures, such as metamaterials or FSS, allowing for the determination of whether these structures possess left-handed properties, where waves propagate backward. Because of the periodicity of the structure and its theoretically infinite extent, Floquet's theorem (or Bloch's wave theorem) states that the outgoing field differs from the incoming field only by a phase factor, which is described by an exponential term. This is represented in the dispersion diagram, where the relationships between the frequency and wave number of the propagating modes reflect this periodicity.. The slope of the straight line connecting the origin to a point on the k - β curve represents the phase velocity V_p, while the slope of the tangent to the curve at that point represents the group velocity V_g. If the phase velocity and the group velocity point in the same direction, it is known as a forward wave (FW). Viceversa, it is known as a backward wave (BW). For the analysis of 1D/2D periodic structures, the Brillouin diagram is used. This diagram identifies propagation zones by clustering propagation directions. The irreducible Brillouin zone for the studied structures is a triangular wedge, determining the full Brillouin zone. This zone includes all possible propagation directions and phase constants along the x and y directions [18]. In Figure 2.5 is shown how the triangular area is selected for this zone, and that is used to optimize a square patch.

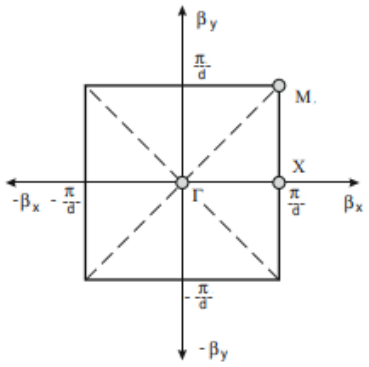

Figure 2.5: Brillouin zone of any geometry with symmetries [18].

In Figure 2.5 "d" denotes the geometrical dimension of the unit cell. To study the 2D square patch using DD there are three possible steps, when the frequency dispersion of the wave phase variations Γ - X, X - M, and M - Γ.

1. Γ - X, it defines the phase constant along x-axes, or it is the base of the Brillouin triangle. It varies from 0 to 180°, while y-direction is fixed at 0 degrees. This is actually what was used in this thesis.

2. X - M, set the phase difference in the x-direction at 180° fixed, and the y-direction varies from 0 to 180°.

3. M - Γ, both the segments are varied that are Γ-X and X-M from 180° to 0.

Chapter 3

Design description and simulation settings

3.1 Simulation Tool

The tool used in this thesis to perform both design and numerical analysis is CST Studio Suite®.
This high-performance 3D EM analysis software is used in the design, analysis, and optimization of EM systems and components. It includes EM field solutions for applications across the EM spectrum in a single user interface. Engineers may study whole systems consisting of several components in an effective and simple manner by coupling the solvers to perform hybrid simulations. The performance and efficiency of antennas and filters, EM compatibility and interference (EMC/EMI), human exposure to EM fields, electro-mechanical effects in motors and generators, and thermal effects in high-power devices are common topics of EM analysis [20].

3.2 Design of a Unit Cell

3.2.1 Configuration 1

The first unit cell can be considered the mother configuration, since all subsequent configurations were obtained by applying some modifications to it. Since, the frequency response of the structure depends on the geometry, it was important to determine the size of the unit cell. The unit cell consisted of a FR-4 substrate layer, with $\epsilon = 4.3$ and $\tan\delta = 0.025$, on which rests metallic rectangular-shaped loadings consisting of PEC. In contrast, the shape of the substrate was square with sides $Du = Dv = 18$ mm and thickness $h1 = 1.58$ mm.
As shown in Figs. 3.1 and 3.2, the unit cell was composed of three resonators, with three different resonant frequencies: two rings, one outer and one inner, and a central cross-shaped one connected by microstrip lines.

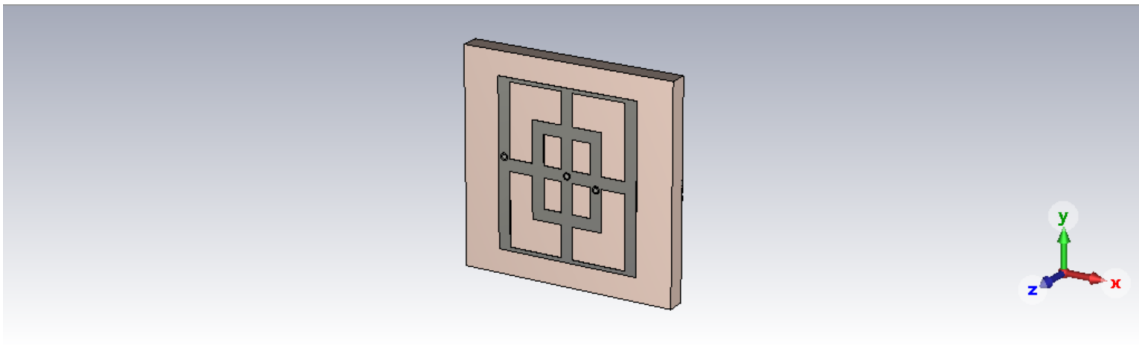

Figure 3.1: Perspective view of Configuration 1 of the unit cell.

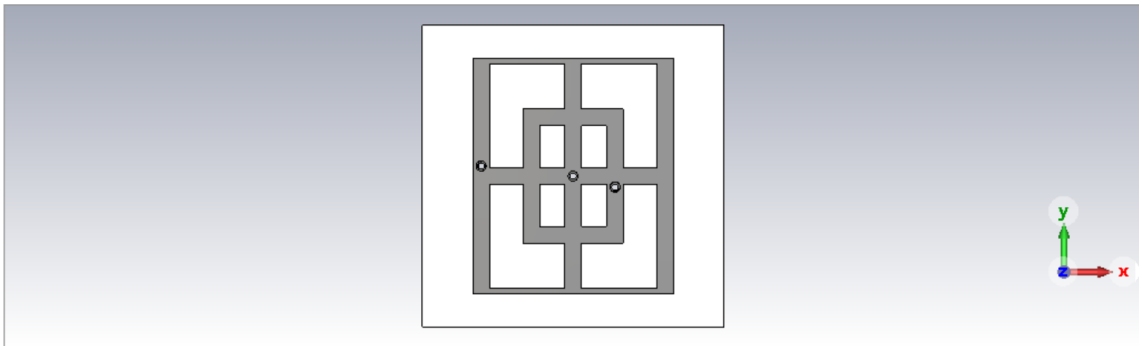

Figure 3.2: Front view of Configuration 1 of the unit cell.

The outer ring resonator was designed with a width (along the x-axis) $xs = 12$ mm and height (along the y-axis) $ys = 14$ mm and a thickness (along the z-axis) $d = 0.035$ mm, instead the inner ring resonator with a width (along the x-axis) $xss = 6$ mm and height (along the y-axis) $yss = 8$ mm with the same thickness d. The central cross-shaped microstrip was designed with a width $ym = 1$ mm and extended to the outer ring intersecting the inner ring. In this way, the unit cell was made to achieve symmetry in both incident planes yoz and xoz.
The symmetry of this structure was broken by the introduction of three metalized vias, with an outer radius $ro1 = 0.3$ mm and an inner radius $ri1 = 0.2$ mm, that were intended to connect the top side with the bottom side, as shown in Fig. 3.3 (oriented alog z-axis), where there are three microstrip lines, having the role of biasing active elements inserted in the cuts (which were not present in this configuration). In this configuration, since all conductors were short circuited, only one conductor was present.

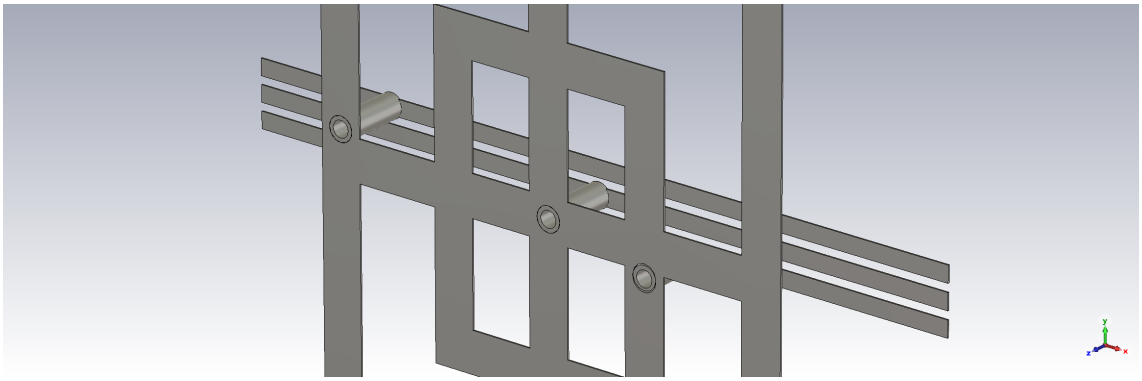

Figure 3.3: Perspective view of the three vias.

As depicted in Fig. 3.4, the microstrip lines extended along the entire unit cell substrate (along the x-axis) with a width $Ld1 = 0.4$ mm and a thickness d, equal to that of the resonators. Each microstrip line was distanced by $gm2 = 0.2$ mm from the next one

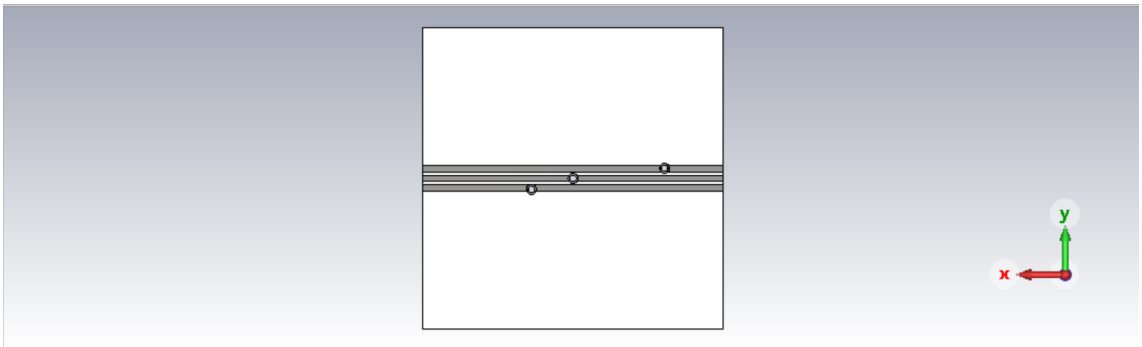

Figure 3.4: Back view of Configuration 1 of the unit cell.

3.2.2 Configuration 2

As anticipated, all other configurations were obtained by applying minor modifications: in particular, for Configuration 2, eight cuts were applied to the microstrip lines in a symmetrical manner, as can be noticed from the Figs. 3.5 and 3.6.
The first four cuts were placed on the cross-shaped microstrip line between the outer and inner rings, while the other four cuts were placed on the same microstrip, but inside the inner ring. The size of each cut is the same $dc = 0.35$ mm, and was intended to disconnect the conductors from each other, creating open circuits. A total of three conductors were obtained. Moreover, no changes were applied regarding the substrate and the microstripes in the bottom side compared to the configuration reported in Fig. 3.4.

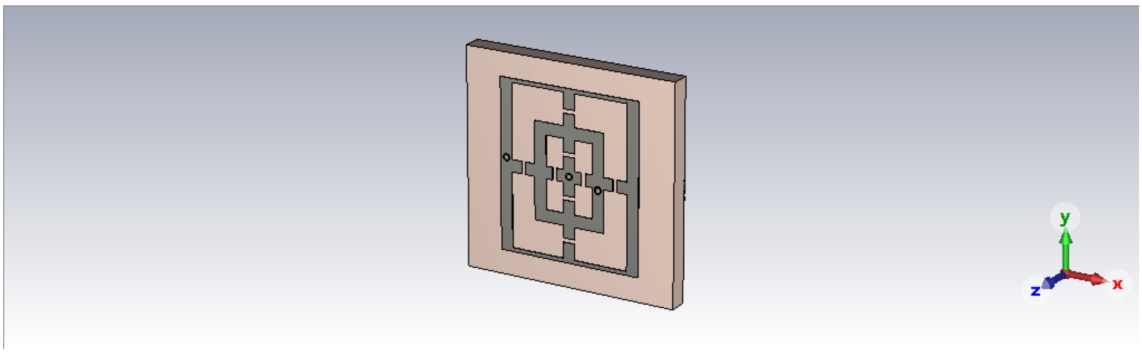

Figure 3.5: Perspective view of Configuration 2 of the unit cell.

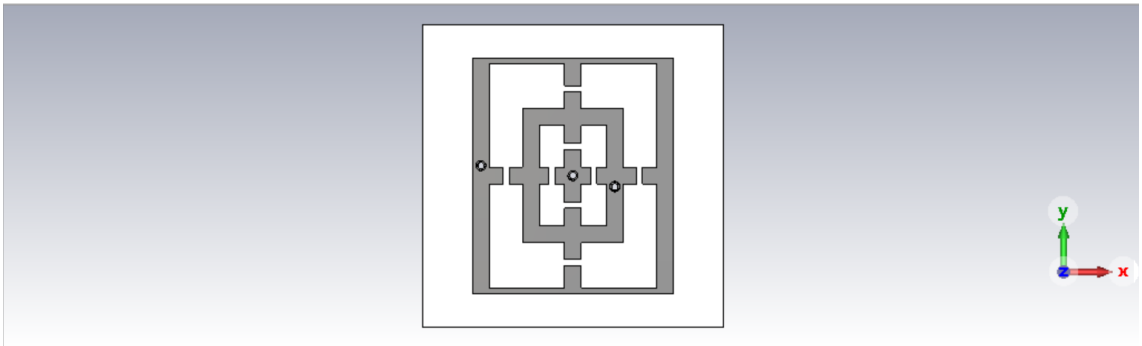

Figure 3.6: Front view of Configuration 2 of the unit cell.

3.2.3 Configuration 3

The same work was done on Configuration 3. In this case, only four cuts were applied. Which precisely were made exclusively in the cross-shaped microstrip line between the outer and inner rings. It is possible to appreciate the configuration in Figs. 3.7 and 3.8.
As before the cut size is the same *dc*. No changes were made to the substrate and microstrip lines placed in the bottom side compared to the Fig. 3.4. Only two conductors were present in this configuration, as the short circuit between the cross-shaped internal microstrip and the inner ring was maintained.

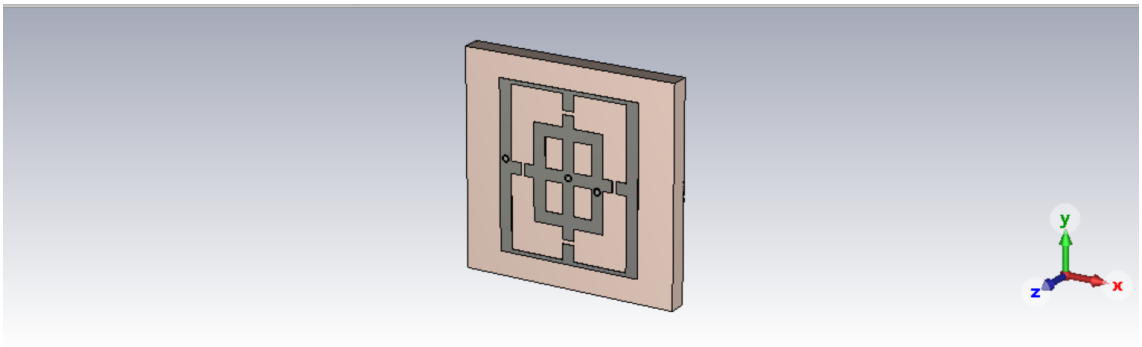

Figure 3.7: Perspective view of Configuration 3 of the unit cell.

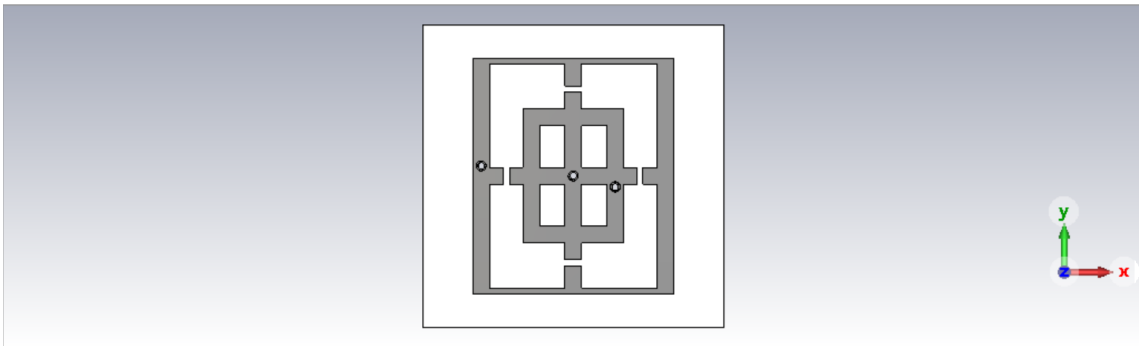

Figure 3.8: Front view of Configuration 3 of the unit cell.

3.2.4 Configuration 4

Finally, Configuration 4 was designed. Just as the previous configurations were applied cuts, in this last case there were four placed again on the cross-shaped microstrip, but internally on the inner ring. Also in this last case the size of the cut is the same *dc*. It is possible to observe the configuration in the Figs. 3.9 and 3.10. Again, no changes were applied to the substrate let alone the microstrip positioned in the bottom side compared to the Fig. 3.4. To conclude also in this last configuration only two conductors were present.

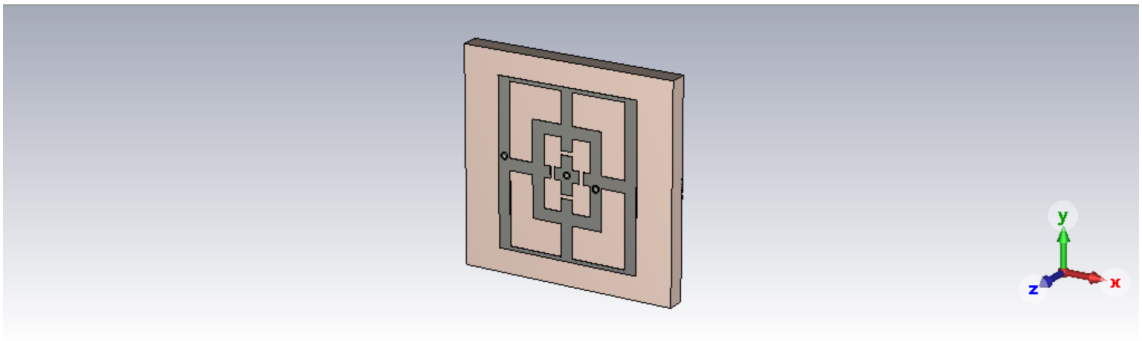

Figure 3.9: Perspective view of Configuration 4 of the unit cell.

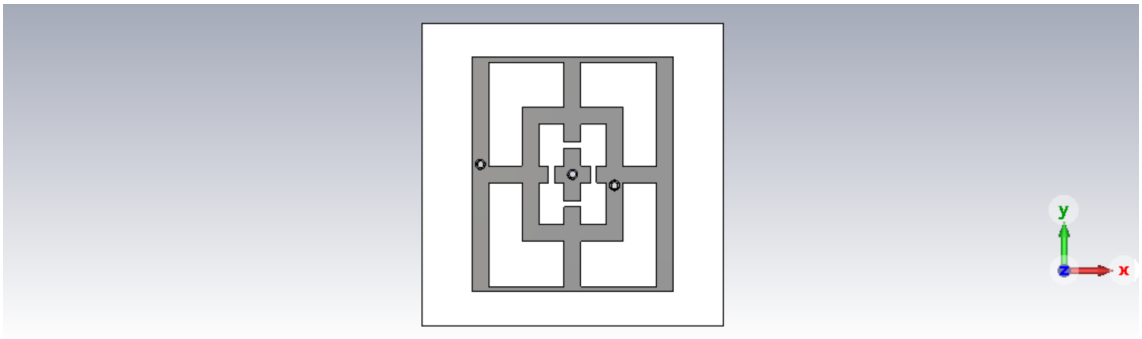

Figure 3.10: Front view of Configuration 4 of the unit cell.

All parameters used in the design phase have been summarized in the Tab. 3.1

Table 3.1: Summary of parameters used in the design

Parameter	Value [mm]	Description
Du	18	Substrate width
Dv	18	Substrate height
h1	1.58	Substrate thickness
xs	12	Outer ring resonator width
ys	14	Outer ring resonator height
d	0.035	Resonator's thickness
xss	6	Inner ring resonator width
yss	8	Inner ring resonator height
ym	1	Central cross-shaped microstrip line width
ro1	0.3	Outer radius metalized vias
ri1	0.2	Inner radius metalized vias
Ld1	0.4	Microstrip line width on the bottom side
gm2	0.2	Microstrip line distance from each other on the bottom side
dc	0.35	Cuts length

3.3 Configuration settings

3.3.1 DD configuration settings

In order to perform a proper analysis and identification of the propagation modes that should have propagated on the surface of the unit cell, an air gap was inserted on both the top and bottom sides. The thickness of the inserted air gap was three times the thickness of the unit cell, as can be observed in the Fig. 3.11. To prevent the air gap and unit cell from overlapping, a boolean function of type "insert" was applied.

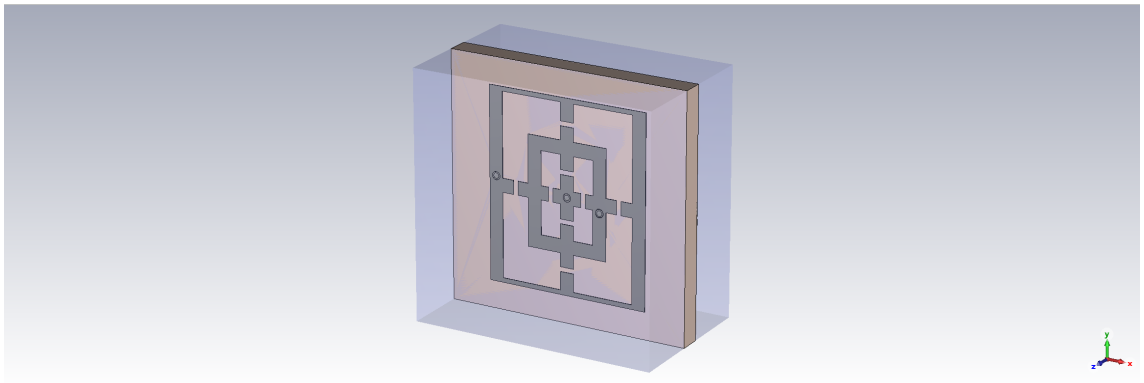

Figure 3.11: Perspective view of the unit cell with the air gap.

Next, the Background properties, Frequency range settings and Boundary conditions had to be set. The background properties were left with the default value proposed by the software, as can be seen in the Fig. 3.12a. In the frequency range settings a min frequency of 0 and a max frequency of 15 GHz was set, as shown in the Fig. 3.12b.

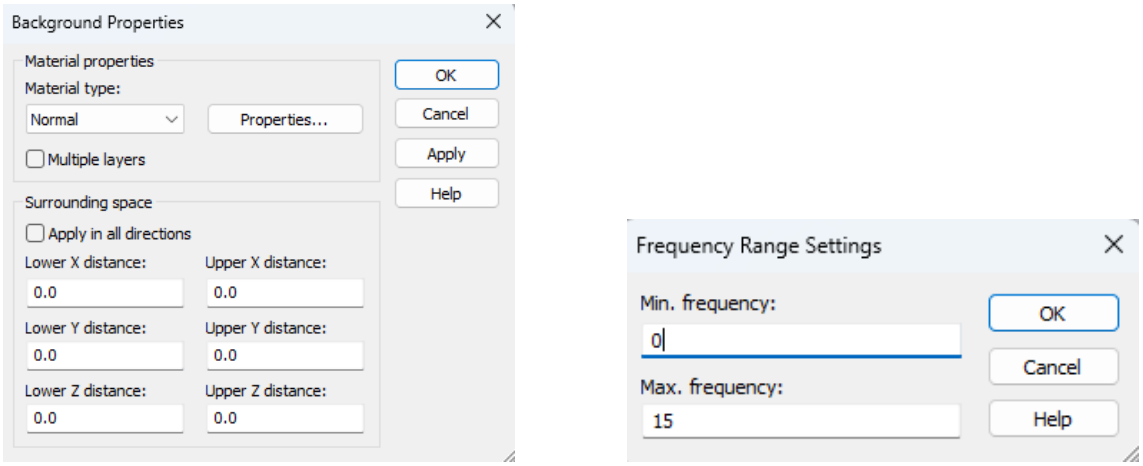

(a) (b)

Figure 3.12: (a) Background properties and (b) Frequency range settings.

More complex, however, was the boundary conditions, as the software did not allow the perfectly matched layer condition to be used in conjunction with Eigenmode solver. Therefore, a different approach was adopted. For the x- and y-direction the Periodic boundary condition was applied, since along this *xoy* plane we wanted to take advantage of the periodicity of the structure. Whereas along the z-direction it was necessary to apply every possible combination of Zmin and Zmax between the two boundary conditions Electric (Et=0) and Magnetic (Mt=0). These boundary conditions specify how the electric and magnetic fields behave on the edges of the domain, respectively.
In detail, for Electric (Et=0) it is assumed that the electric field cannot have a tangential component along the surface. This boundary condition is often used to simulate a Perfect Electric Conductor (PEC) conductive wall.
Whereas, Magnetic (Mt=0) indicates that the magnetic field tangential to the boundary surface is null. It is used to simulate a Perfect Magnetic Conductor (PMC) conductive wall [20].
Simulations were then carried out with each combination of boundary conditions: PEC-PEC, PEC-PMC, PMC-PEC, PMC-PMC. All the combinations of boundary conditions analyzed are shown in the Figs. 3.13, 3.14, 3.15 and 3.16.

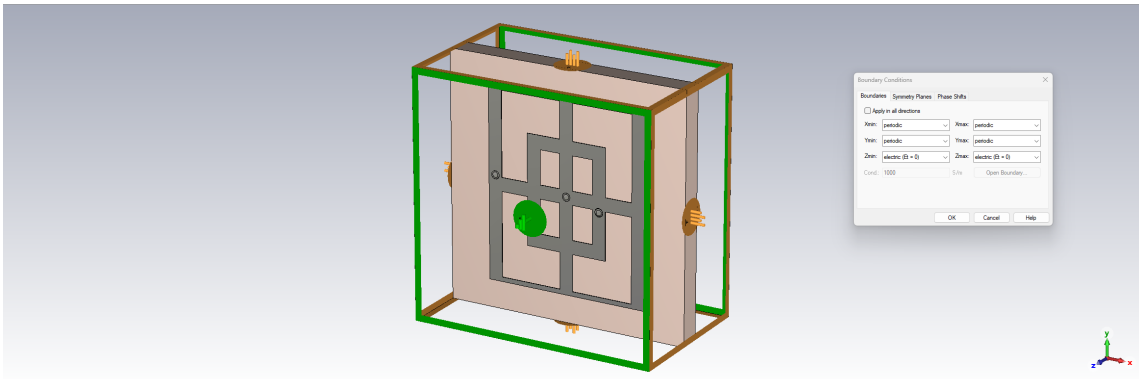

Figure 3.13: Combination 1: PEC-PEC.

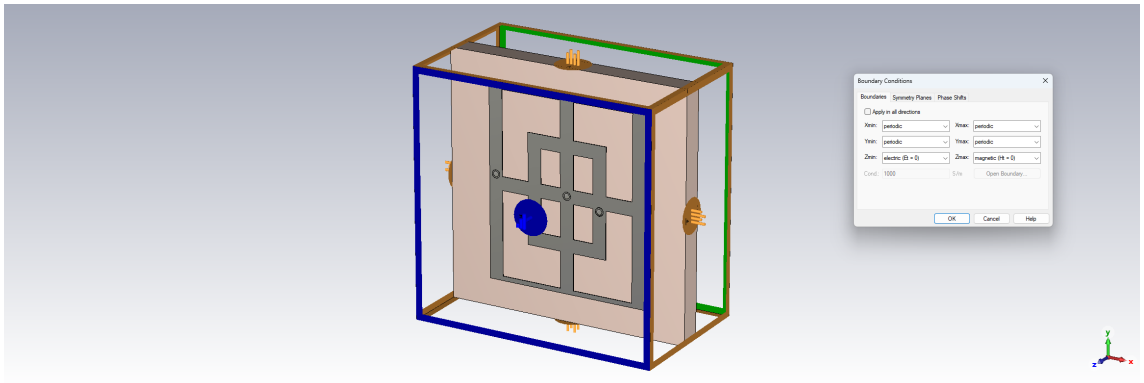

Figure 3.14: Combination 2: PEC-PMC.

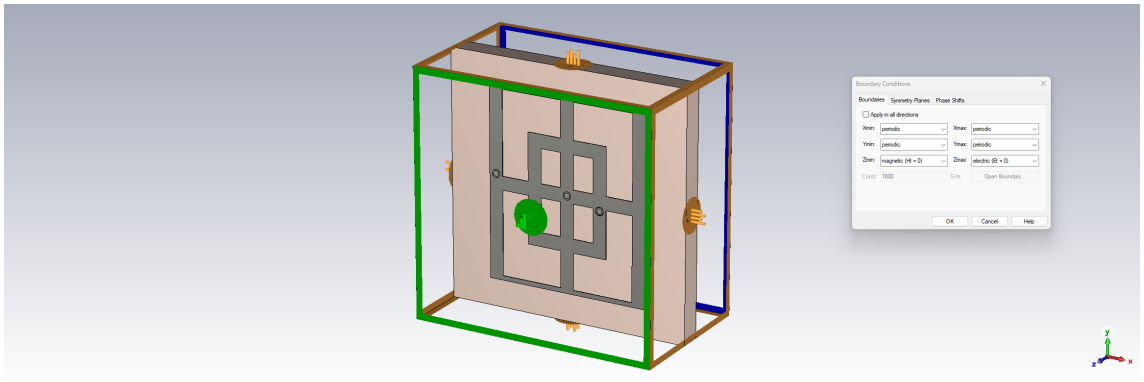

Figure 3.15: Combination 3: PMC-PEC.

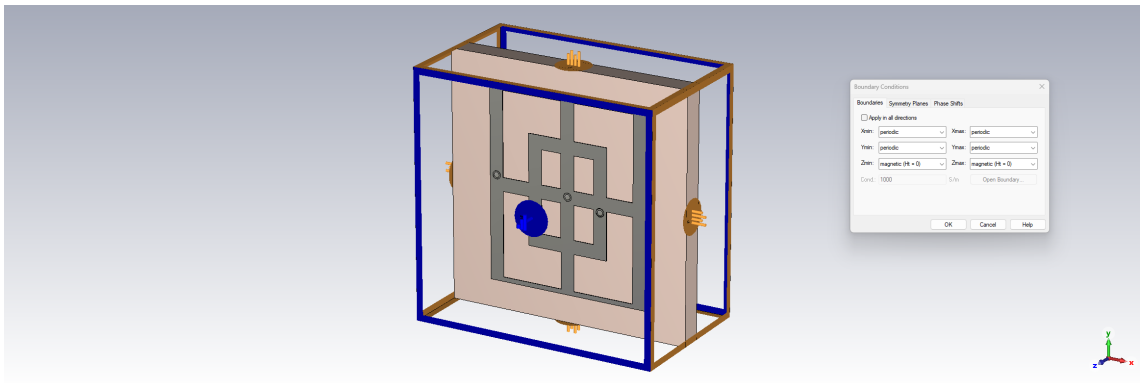

Figure 3.16: Combination 4: PMC-PMC.

The next step was to set the Phase Shift in the boundary conditions. A *px* parameter was set, to which a parametric sweep was then applied. Shown in the Fig. 3.17 is how this was done.

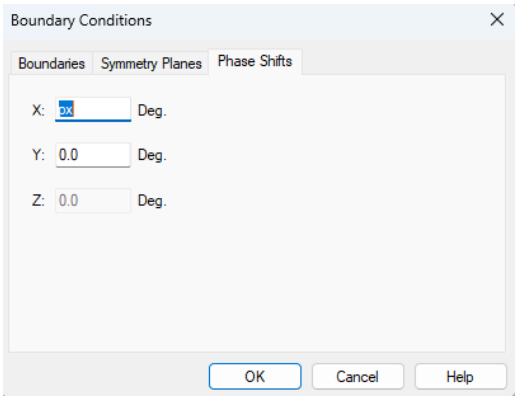

Figure 3.17: Phase shift in boundary condition.

To obtain the DD, the appropriate solver was selected: Eigenmode Solver. At this point, launching the solver opened the window shown in the Fig. 3.18 and the fields related to Solver setting were changed.

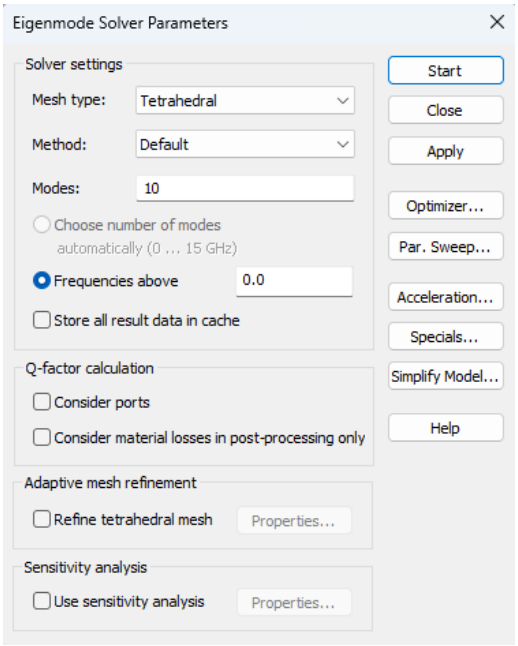

Figure 3.18: Eigenmode Solver window.

In particular the Mesh type was set Tetrahedral, Method as Default and Mode equal to 10, as it was decided to get ten propagation modes (of increasing frequency). All other fields were left as default. Finally, the Adaptive mesh refinement field was decided, as a preliminary analysis, not to be selected. This is because given the high computational cost of the simulation to start with a rougher approach and lower mesh granularity made it possible to speed up the initial study of the phenomenon, and then proceed with a more in-depth and expensive analysis.
To launch the simulation we then had to apply Parametric Sweep to the *px* parameter as shown in the Fig. 3.19. A new sequence was then created with a parametric sweep of linear type from the phase value of 4.5 to 175.5, just to avoid the calculations near the band edges, with a step width of 9. In this way, 20 points were obtained with which to calculate each curve representing the frequency of propagation modes as the phase difference varies.

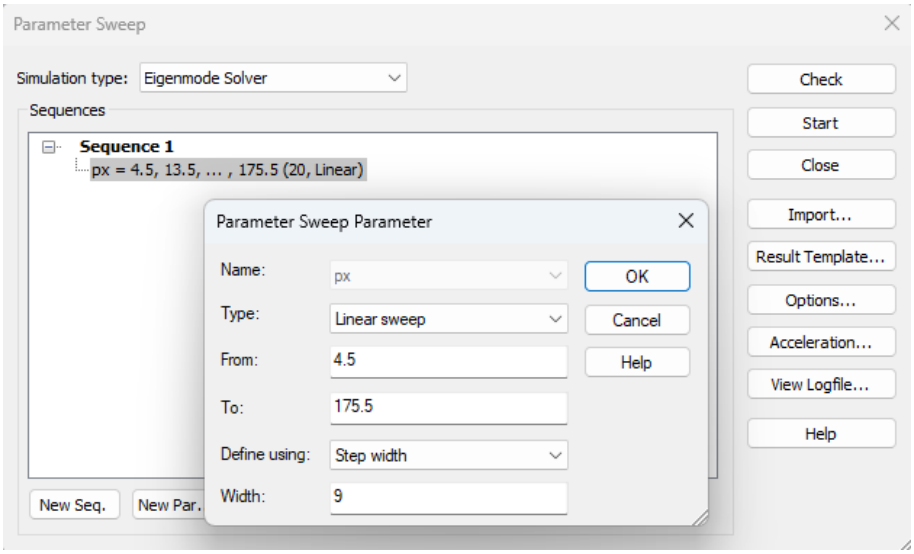

Figure 3.19: Parametric sweep window for the DD.

3.3.2 S-Matrix configuration settings

In order to properly carry out and analyze the simulations related to the Scattering parameters, some settings had to be revised from the previous case. The Background properties and Frequency range settings were set identically from the previous DD simulation.
While different is the matter related to the boundary conditions, in fact it was not necessary to analyze four different cases. Along the x- and y-direction the Unit Cell boundary condition was applied, as it assumes that the simulated structure repeats periodically in space. While along the z-direction the Open (Add Space) boundary condition was applied as it adds a layer of space around the simulated structure, which allows the EM field to disperse as if it were in an infinite environment. This condition avoids artificial reflections from the edges of the simulation domain, which could distort the results. The boundary conditions applied are shown in the Fig. 3.20.

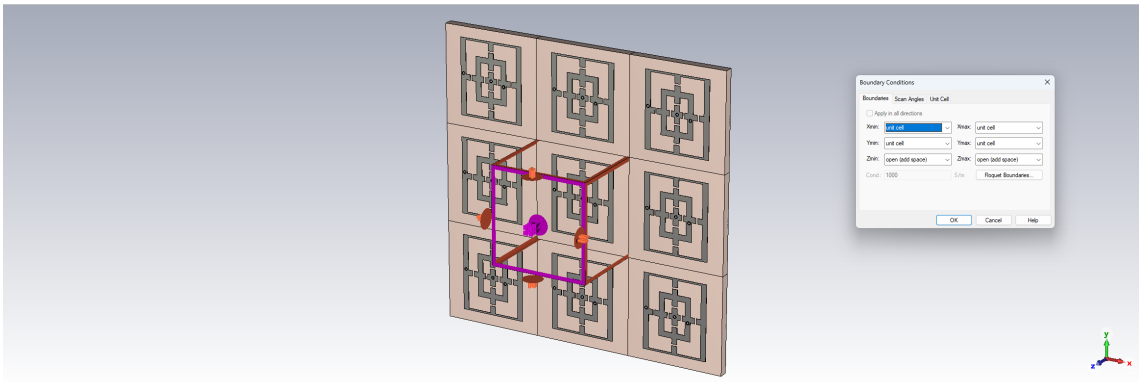

Figure 3.20: Boundary conditions applied in the case of S-Matrix simulation.

The next step was to set the scan angle in the boundary conditions. Two parameters were set ϕ and θ, which represent the two angles in the spherical coordinates. The ϕ was set to 0, while a parametric sweep was then applied on θ. Fig. 3.21 shows how it was done.

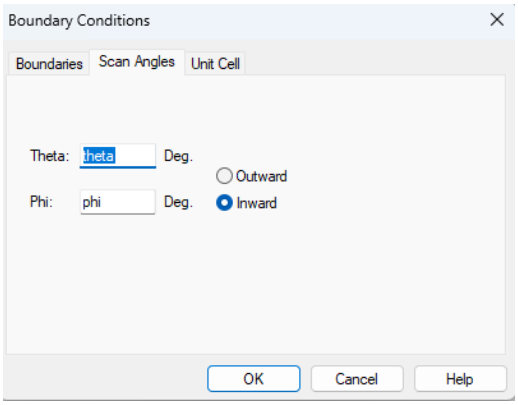

Figure 3.21: Scan angles in Boundary conditions.

Next, the Floquet port was set up.
A Floquet port exploits the concept of Floquet waves, which are solutions of Maxwell's equations for periodic structures. Floquet ports facilitate the analysis of transmittance (how much of the incident power is transmitted through the structure) and reflectance (how much is reflected).
The number of Floquet modes was set to 2, while all other fields were set as default, as shown in Fig. 3.22.

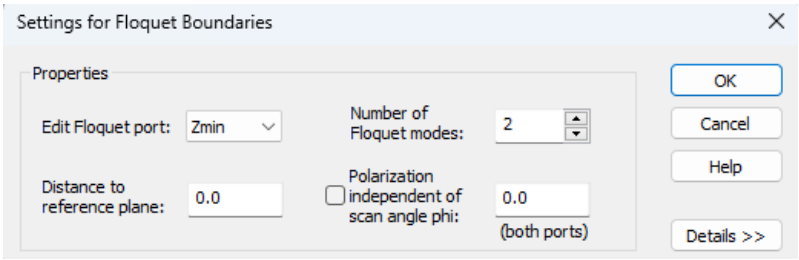

Figure 3.22: Floquet port settings.

For obtaining the transmittance plot, the appropriate solver was selected: Frequency Domain Solver. At this point, launching the solver opened the window shown in the Fig. 3.23 and the fields related to Solver setting were checked. All fields were set as default.
In particular, however, compared with the DD case, the box for adaptive tetrahedral mesh refinement was immediately checked because the computational cost of such a simulation is significantly lower.

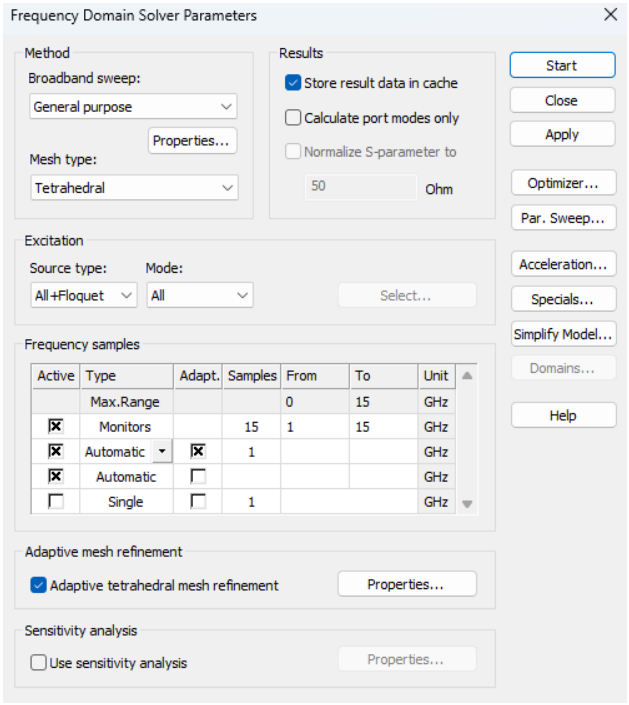

Figure 3.23: Frequency Domain Solver window.

To launch the simulation, we then applied a Parametric sweep to the parameter θ as shown in the Fig. 3.24. A new sequence was then created with a parametric sweep of linear type with θ varying from 0 to 45° with a step width of 15°. In this way four different incidences are analyzed: 0, 15°, 30° and 45° so as to analyze how the S-Matrix varies as the angle of incidence varies.

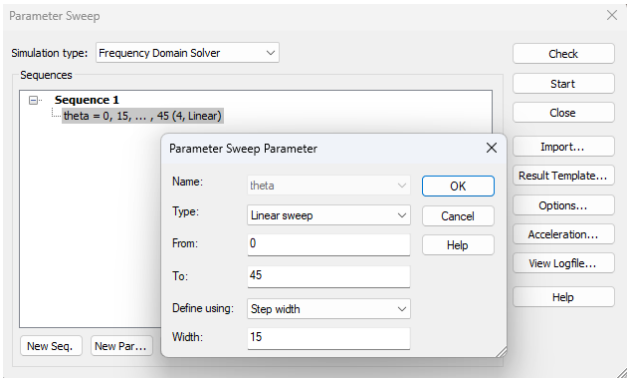

Figure 3.24: Parametric sweep window for the S-Matrix.

Chapter 4

Final results

4.1 Analysis of surface propagation modes

Once the DD simulation was finished, many results related to propagation modes were obtained. The first analysis was performed on the electric field distribution in the unit cell. Electric field distribution refers to the description of how the electric field varies in space. This field is a vector quantity that represents the force that an electric charge exerts on other charges in the surrounding space. It can be determined by charge sources and Maxwell's laws [21, 10]. The distribution of the electric field can be represented graphically by field lines, which show the direction of the field at various points in space, and the density of these lines indicates the strength of the field [21].
For brevity, three different examples of electric field distributions were given below related to the configuration 1.
The first, represented in Figs. 4.1 and 4.2 showed how the electric field is distributed in vector form and absolute value respectively in mode 1 of the unit cell configuration 1. It was noted that this mode was distributed more in the inserted air gap. This allowed us to exclude it, as our analysis focused on the modes concentrating in the dielectric so as to excite the surface-applied resonators.

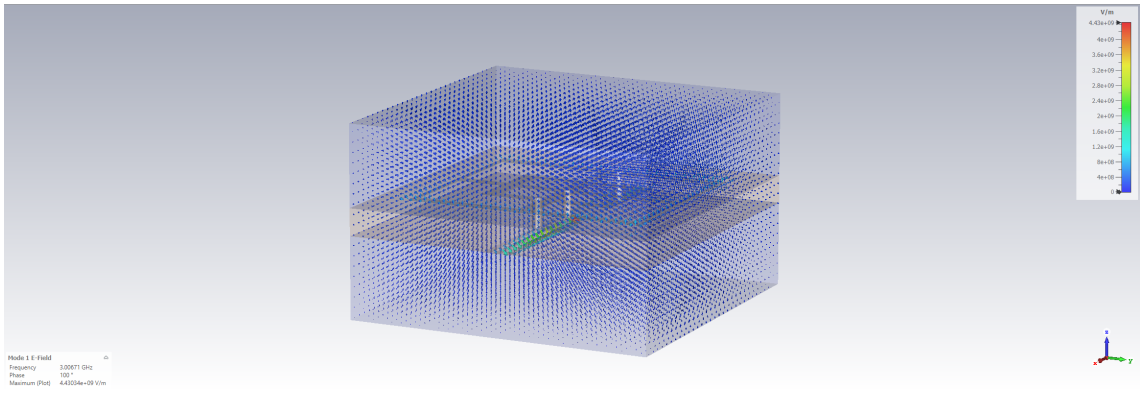

Figure 4.1: Electric field distribution vector form Configuration 1 mode 1.

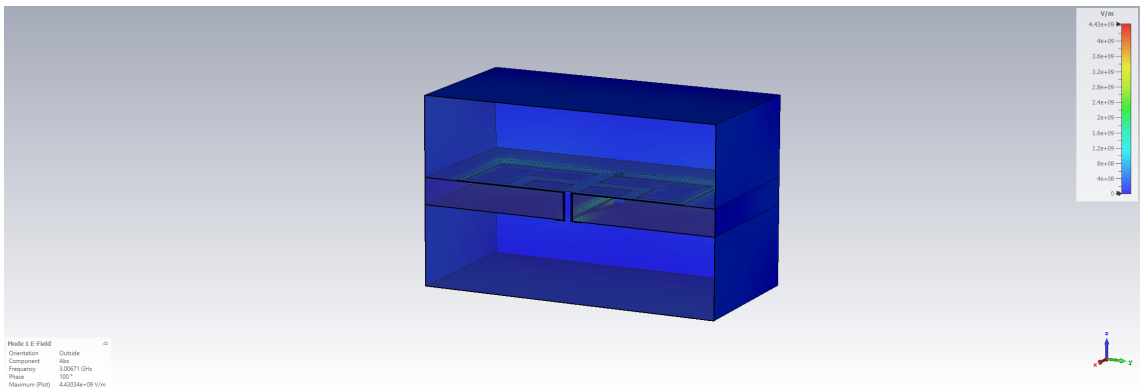

Figure 4.2: Electric field distribution absolute value Configuration 1 mode 1 (Cutting plane along x-axis).

The second example, represented in Figs. 4.3 and 4.4 showed how the electric field is distributed in vector form and absolute value respectively in mode 4 of the unit cell configuration 1. It was noticed that this mode was distributed more on the microstrip lines located in the bottom side of the unit cell. In contrast to the previous example, here the electric field was almost not distributed at all in the air gap, and this was asserted by looking at the density of field lines present outside the structure. This type of mode was accepted for the study.

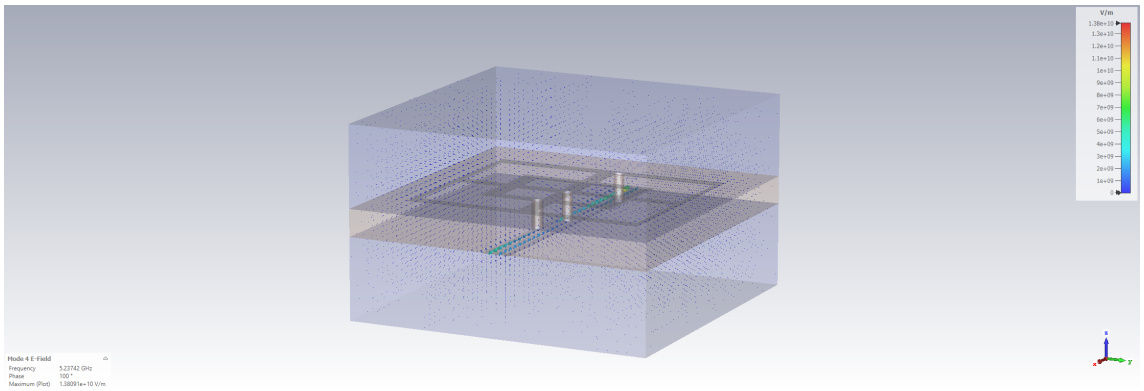

Figure 4.3: Electric field distribution vector form Configuration 1 mode 4.

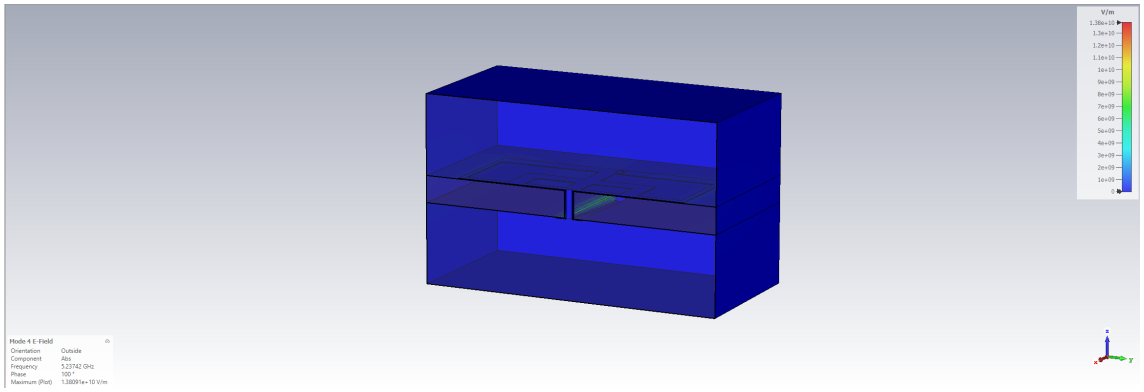

Figure 4.4: Electric field distribution absolute value Configuration 1 mode 4 (Cutting plane along x-axis).

The third example proposed, represented in Figs. 4.5 and 4.6 showed how the electric field is distributed in vector form and absolute value respectively in mode 9 of the unit cell configuration 1. Unlike the previous two examples, this mode was found to concentrate a lot on the outer resonator ring. Furthermore, this mode did not particularly distributed in the air gap, so it could be asserted that it concentrated in the dielectric, so this type of mode was considered in the study.

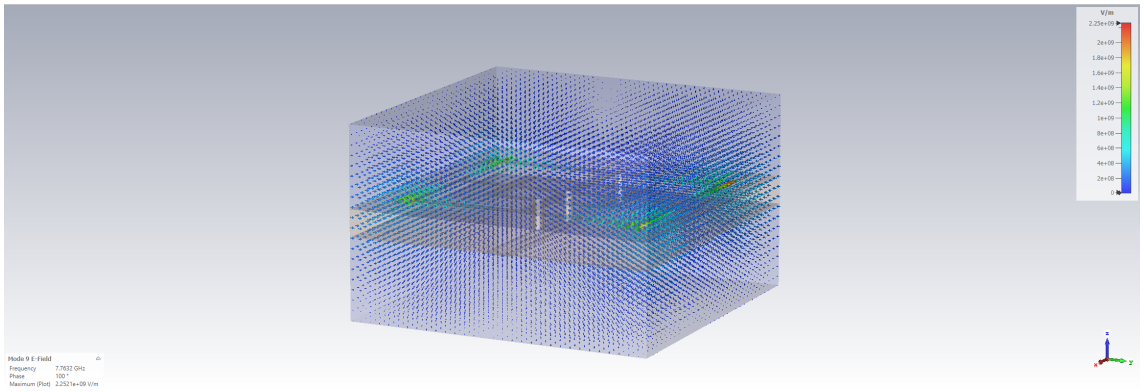

Figure 4.5: Electric field distribution vector form Configuration 1 mode 9.

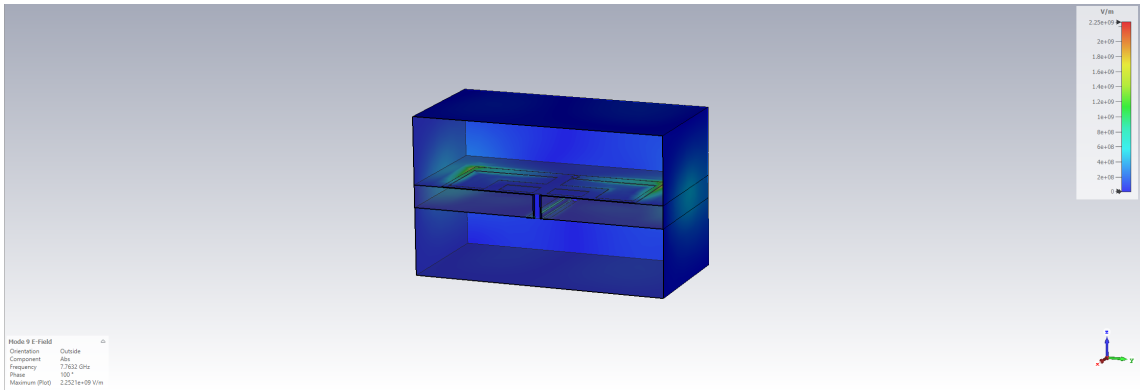

Figure 4.6: Electric field distribution absolute value Configuration 1 mode 9 (Cutting plane along x-axis).

4.2 Dispersion Diagram analysis

Next, the DDs of the four different unit cell configurations in the four different cases of PEC-PEC, PEC-PMC, PMC-PEC, PMC-PMC boundary conditions were analyzed. For each combination, 10 different modes were obtained in according with the configuration set on the Eigenmode Solver. Due to the similarity of the results, only two examples have been reported, namely the DD of configuration 1 case PEC-PEC and the DD of configuration 2 case PMC-PMC.
It was possible to see that the different modes with increasing frequency had different behaviors as the *px* phase difference increased. In particular, it was noted that there were modes that increased in frequency as the phase difference increased, others decreased as the phase difference increased, and others intersected with other modes. Finally, it was noticed that some modes maintained an almost constant frequency response as the phase difference increased.
It further needs to be considered that these behaviors were also influenced to a small extent by the restrictions related to the number of applicable meshes and the FR4 (lossy) material applied as a substrate. By having a computer that can support a higher computational load, the results obtained could be more accurate. In Figure 4.7 is shown the DD of the configuration 1 case PEC-PEC, instead in Fig. 4.8 is shown the DD of the configuration 2 case PMC-PMC.

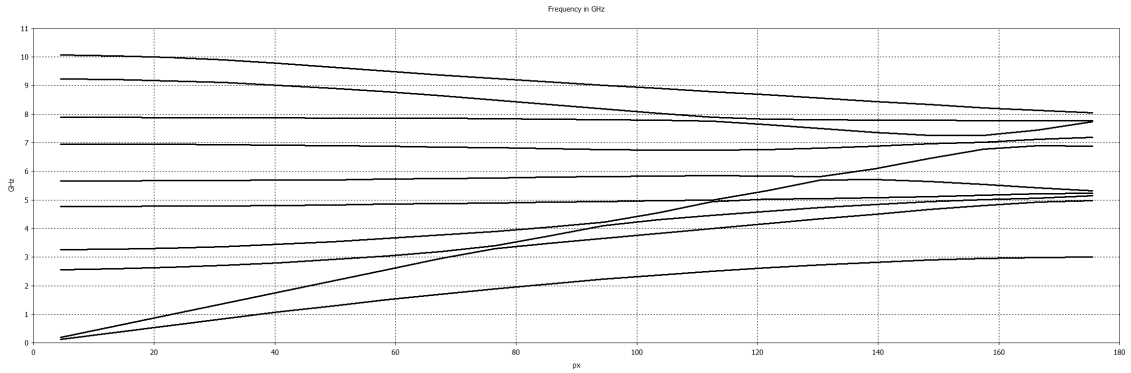

Figure 4.7: Dispersion Diagram configuration 1 of the unit cell case PEC-PEC.

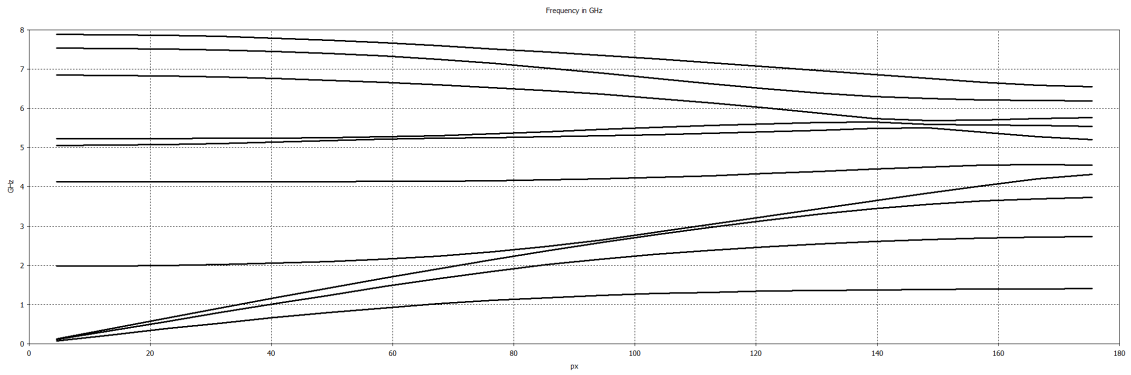

Figure 4.8: Dispersion Diagram configuration 2 of the unit cell case PMC-PMC.

4.3 S-Matrix Analysis

In this section, the scattering parameters of the four different configurations were analyzed. Each scattering parameter was calculated by applying four different angles of incidence θ (0, 15°, 30°, 45°) in accordance with the configuration set on the frequency domain solver. This analysis was carried out to study the effect that this angle affects the transmittance and reflectance of a periodic structure. Noting that the effect obtained was similar on each configuration, it was decided, for the sake of brevity, to report in this thesis only the results obtained on configurations 1 and 2 so as to maintain consistency with the results reported of the DD.
Shown in Figs. 4.9 and 4.10, respectively, the S12 and S11 parameters of the S-matrix of configuration 1. It was noted that the various dips present in both the transmission coefficient and reflection coefficient are frequency shifted as the applied angle of incidence changes. In particular, two different types of frequency shift patterns were found: the frequency of the dips increases proportionally with the angle of incidence or the frequency of the dips decreases proportionally as the angle of incidence increases. Furthermore, in the S11 parameter in Fig. 4.10, it was observed that at the matching frequency $f = 5$ GHz there was a dip with almost zero frequency shift.

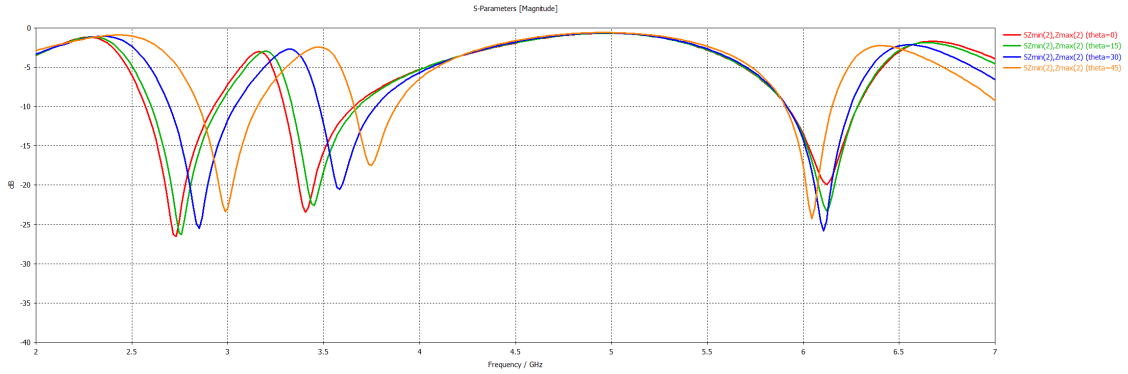

Figure 4.9: Scattering parameter S12 for the Configuration 1 of the unit cell.

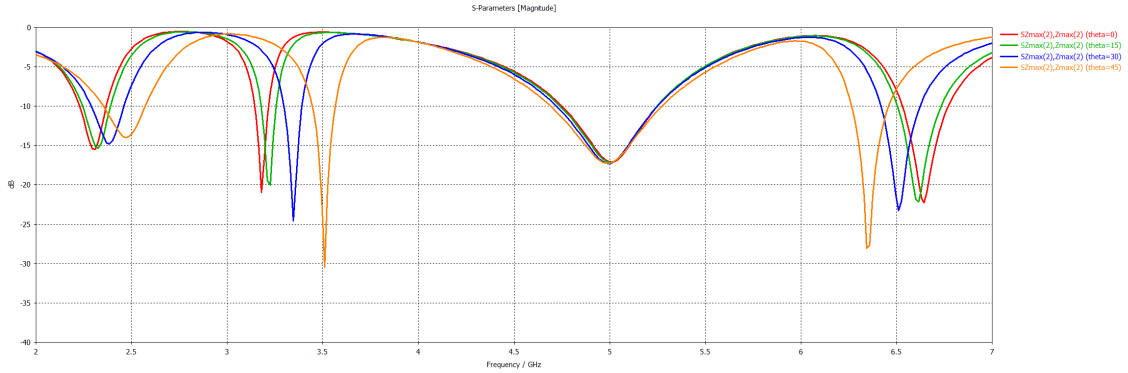

Figure 4.10: Scattering parameter S11 for the Configuration 1 of the unit cell.

As anticipated, the same frequency shift pattern also occurred for the scattering parameters in configuration 2. In Figures 4.13 and 4.14 are shown the S12 and S11 parameters for the unit cell with configuration 2.

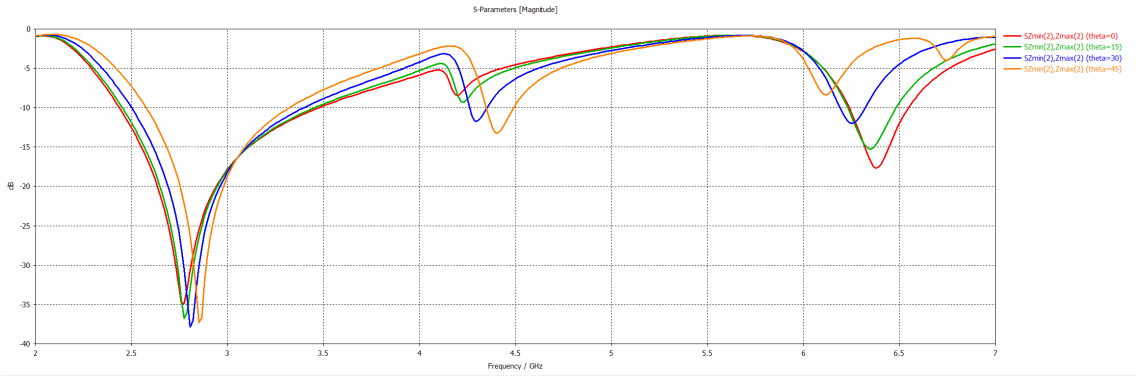

Figure 4.11: Scattering parameter S12 for the Configuration 2 of the unit cell.

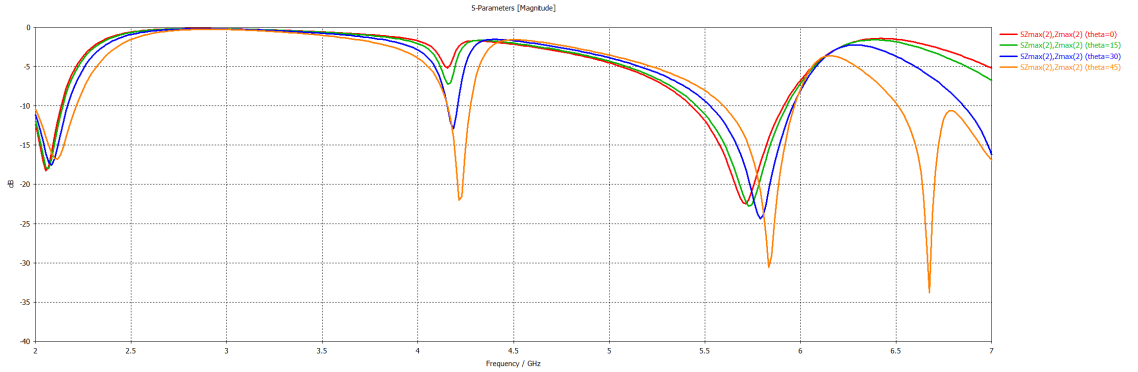

Figure 4.12: Scattering parameter S11 for the Configuration 2 of the unit cell.

4.4 Comparison between Scattering parameters and DD

Finally, a comparison was made between the results obtained from the DD and Scattering parameters. In particular, the connection between the modes that concentrated in the dielectric and the transmittance/reflectance of the unit cell was studied. For brevity, only configuration 1 was considered in this analysis, for DD in the PEC-PEC case, and the S-Matrix result of the S11 parameter for the same configuration. From the two graphs shown in Figs. 4.13 and 4.14, it was possible to define a strong correlation between the slope of the modes in the DD and the frequency shift analyzed in the scattering parameters. It could be asserted that if the slope of the curve describing the mode in DD is positive (increasing frequency as the phase variation increases) then a positive frequency shift is obtained in the scattering parameter as the angle of incidence increases. Conversely, if the slope of the curve describing the mode in DD is negative (decreasing frequency as the phase variation increases) then a negative frequency shift is obtained in the scattering parameter as the angle of incidence increases. Finally, if the slope is flat (constant frequency as the phase variation increases) then no frequency shift is obtained as the angle of incidence increases.

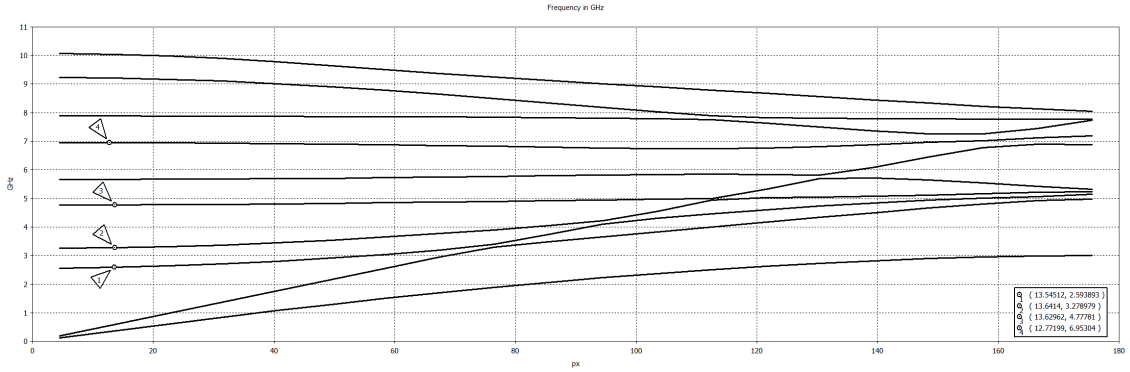

Figure 4.13: Dispersion Diagram configuration 1 of the unit cell case PEC-PEC.

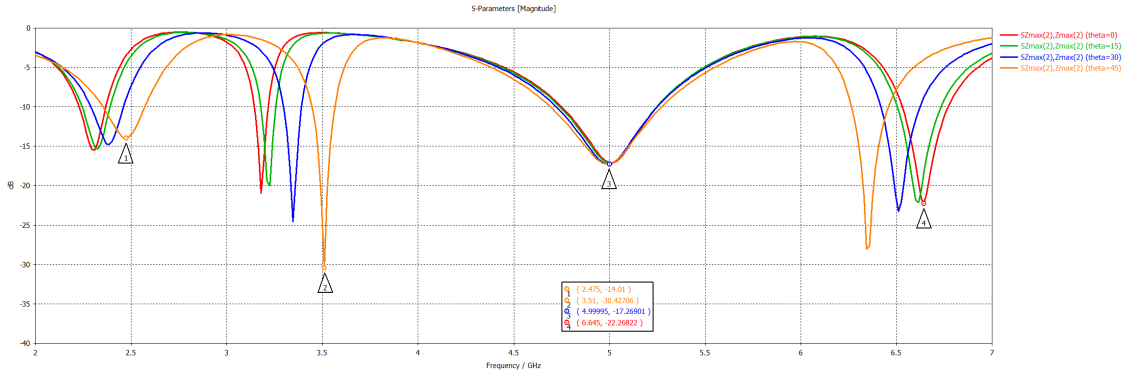

Figure 4.14: Scattering parameter S11 for the Configuration 2 of the unit cell.

Focusing on the three different cases of frequency shifts present in Fig. 4.15, Tab. 4.1 was created, in which all the frequency dip values of the S11 parameter and the relative frequency shifts present were collected.

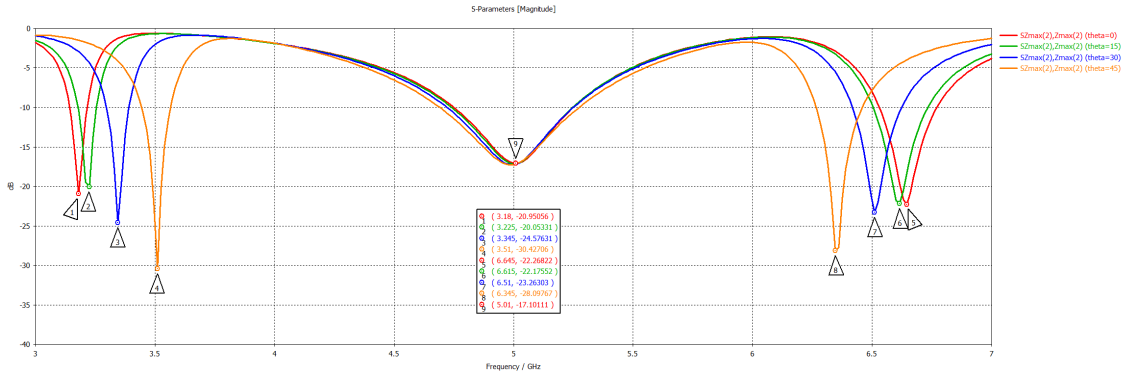

Figure 4.15: Scattering parameter S11 for the Configuration 2 of the unit cell with frequency markers.

Table 4.1: Summary of frequency shift in S11 for different slopes in DD.

Slope	f_0 [GHz]	f_1 [GHz]	f_2 [GHz]	f_3 [GHz]	Δf_1 [GHz]	Δf_2 [GHz]	Δf_3 [GHz]
Positive	3.180	3.225	3.345	3.510	0.045	0.120	0.165
Negative	6.645	6.611	6.510	6.345	-0.034	-0.101	-0.165
Constant	5.010	5.000	4.995	4.995	-0.010	-0.005	0

where f_0 is the dip frequency with angle of incidence $\theta = 0$
f_1 is the dip frequency with angle of incidence $\theta = 15°$
f_2 is the dip frequency with angle of incidence $\theta = 30°$
f_3 is the dip frequency with angle of incidence $\theta = 45°$
$\Delta f_1 = f_1 - f_0$
$\Delta f_2 = f_2 - f_1$
$\Delta f_3 = f_3 - f_2$

Chapter 5

Future works

This thesis has numerically investigated and analyzed surface waves in relation to the transmission properties of tunable periodic structures with particular attention to the DD and scattering parameters. However, there are several interesting directions that can be explored to extend and deepen this work.
One possible extension of this work involves the integration of PIN diodes into the cuts placed on the unit cell structure proposed. Through the implementation of PIN diodes, the structure would be able to selectively transmit or reflect EM waves according to frequency. Future research could focus on advanced numerical simulations and parameter optimization to understand the impact of PIN diodes on the frequency response and maximize the efficiency and responsiveness of the periodic structure [2]. Another crucial step is the practical realization. Collaboration with companies specializing in circuit printing to physically realize the prototype according to the specifications defined by the simulations. This includes choosing materials, printing precision, and verifying tolerances according to the company's construction constraints. After fabricating the prototype, it is essential to conduct accurate experimental tests to evaluate the real performance to compare with those obtained in simulations. Analysis in an anechoic chamber represents an ideal opportunity for this purpose.

Bibliography

[1] C. Caloz and T. Itoh, Electromagnetic Metamaterials: Transmission Line Theory and Microwave Applications. Hoboken, NJ, USA: Wiley, 2006.

[2] B. A. Munk, Frequency Selective Surfaces: Theory and Design. Hoboken, NJ, USA: Wiley, 2000.

[3] J. D. Joannopoulos, S. G. Johnson, J. N. Winn, and R. D. Meade, Photonic Crystals: Molding the Flow of Light. Princeton, NJ, USA: Princeton Univ. Press, 2011.

[4] Farzad Mir, Ladislau Matekovits, Aldo De Sabata, "Symmetry-Breaking Manipulation in the Design of Multifunctional Tunable Frequency Selective Surface," International Journal of Electronics and Communications (AEÜ), vol. 142, 2021, p. 154003. Available online 23 October 2021, https://doi.org/10.1016/j.aeue.2021.154003.

[5] J. B. Pendry, D. Schurig, and D. R. Smith, "Controlling Electromagnetic Fields," Science, vol. 312, no. 5781, pp. 1780–1782, Jun. 2006.

[6] C. L. Holloway, E. F. Kuester, J. A. Gordon, J. O'Hara, J. Booth, and D. R. Smith, "An Overview of the Theory and Applications of Metasurfaces: The Two-Dimensional Equivalents of Metamaterials," IEEE Antennas Propag. Mag., vol. 54, no. 2, pp. 10–35, Apr. 2012.

[7] J. Zhang, L. Li, and M. Wang, "A Study on Advanced Communication Systems," in *2021 International Conference on Advanced Communication and Signal Processing (ACES-China)*, 2021, pp. 123-128. doi: 10.23919/ACES-China52398.2021.9581864.

[8] R. B. Hwang, *Periodic Structures: Mode-Matching Approach and Applications in Electromagnetic Engineering*. Wiley-IEEE Press, 2012.

[9] C. H. Papas, *Theory of Electromagnetic Wave Propagation*. Dover Publications, 2003.

[10] J. D. Jackson, *Classical Electrodynamics*. Wiley, 1998.

[11] N. Engheta and R. W. Ziolkowski, *Electromagnetic Metamaterials: Physics and Engineering Explorations*, Wiley-IEEE Press, 2006.

[12] G. V. Eleftheriades and K. G. Balmain, *Negative-Refraction Metamaterials: Fundamental Principles and Applications*, Wiley-IEEE Press, 2005.

[13] A. P. Sohrab, S. Ahdi Rezaeieh, and K. S. Zainud-Deen, "Flexible and Wearable Frequency Selective Surfaces and Metasurfaces: A Review," *Applied Sciences*, vol. 8, no. 9, p. 1689, Sep. 2018.

[14] C. M. Soukoulis and M. Wegener, "Past achievements and future challenges in the development of three-dimensional photonic metamaterials," *Nature Photonics*, vol. 5, pp. 523-530, 2011.

[15] S. A. Tretyakov, *Analytical Modeling in Applied Electromagnetics*, Artech House, 2003.

[16] S. Narayan and A. Kesavan, (Eds.), *Handbook of Metamaterial-Derived Frequency Selective Surfaces*, CRC Press, 2018.

[17] V. A. Boriskin and S. V. Boriskina, *Micro and Nano Optics: Elements and Systems*, Cambridge University Press, 2010.

[18] R. Kubacki, S. Lamari and K. Rudyk, "The dispersion diagram used for periodic patterned microstrip antenna analysis," in *2016 21st International Conference on Microwave, Radar and Wireless Communications (MIKON)*, Krakow, Poland, 2016, pp. 1-4. doi: 10.1109/MIKON.2016.7492065.

[19] S. J. Orfanidis, *Electromagnetic Waves and Antennas*. Rutgers University, 2016.

[20] Dassault Systèmes, "CST Studio Suite," [Online]. Available: https://www.3ds.com/products/simulia/cst-studio-suite.

[21] D. J. Griffiths, *Introduction to Electrodynamics*. Prentice Hall, 1999.

Acknowledgements

I would like to give special thanks to Prof. Ladislau Matekovits for providing me with all the support I needed to undertake this thesis work. His constant supervision was essential and instructive throughout the whole thesis experience.
I would also like to thank my family for allowing me to have this wonderful opportunity and supporting me throughout this journey.
Finally, I would like to thank all my friends for encouraging me in difficult times to keep going and never give up.